AIAA 98-4569
An Atmospheric Guidance Algorithm Testbed for the Mars Surveyor Program 2001 Orbiter and Lander

Scott A. Striepe, Eric M. Queen, Richard W. Powell,
Robert D. Braun, F. McNeil Cheatwood
NASA Langley Research Center
Hampton, VA

John T. Aguirre
NYMA, Inc.
Hampton, VA

Laura A. Sachi
Lockeed-Martin Astronautics
Denver, CO

Daniel T. Lyons
NASA Jet Propulsion Laboratory
Pasadena, CA

AIAA Atmospheric Flight Mechanics Conference
August 10-12, 1998 / Boston, MA

An Atmospheric Guidance Algorithm Testbed for the Mars Surveyor Program 2001 Orbiter and Lander

Scott A. Striepe,* Eric M. Queen,* Richard W. Powell,* Robert D. Braun,* F. McNeil Cheatwood*
NASA Langley Research Center
Hampton, VA

John T. Aguirre**
NYMA, Inc.
Hampton, VA

Laura A. Sachi†
Lockheed Martin Astronautics
Denver, CO

Daniel T. Lyons‡
NASA Jet Propulsion Laboratory
Pasadena, CA

Abstract

An Atmospheric Flight Team was formed by the Mars Surveyor Program '01 mission office to develop aerocapture and precision landing testbed simulations and candidate guidance algorithms. Three- and six-degree-of-freedom Mars atmospheric flight simulations have been developed for testing, evaluation, and analysis of candidate guidance algorithms for the Mars Surveyor Program 2001 Orbiter and Lander. These simulations are built around the Program to Optimize Simulated Trajectories. Subroutines were supplied by Atmospheric Flight Team members for modeling the Mars atmosphere, spacecraft control system, aeroshell aerodynamic characteristics, and other Mars 2001 mission specific models. This paper describes these models and their perturbations applied during Monte Carlo analyses to develop, test, and characterize candidate guidance algorithms.

Nomenclature

AFT	Mars 2001 Atmospheric Flight Team
ASAP	Artificial Satellite Analysis Program
ATM	Coordinate Frame aligned with Mars Relative Velocity Vector
CF	Climate Factor curve fit coefficients
CFD	Computational Fluid Dynamics
cg	Center of gravity
GCM	Global Circulation Models
IMU	Inertial Measurement Unit
JPL	Jet Propulsion Laboratory
JSC	Johnson Space Center
K_n	Knudsen number
LaRC	Langley Research Center
LAURA	Langley Aerothermodynamic Upwind Relaxation Algorithm
L/D	Lift-to-Drag Ratio
LMA	Lockheed-Martin Astronautics
M	Mach number
MarsGRAM	Mars Global Reference Atmosphere Model
MCI	Mars-Centered Inertial coordinate system
MCMF	Mars-Centered Mars-Fixed coordinate system
MRE	Mars Reference Radius
MSP '01	Mars Surveyor Program 2001
NASA	National Aeronautics and Space Administration
NAV	Quantities calculated from estimated states
PI	Principal Investigator of a guidance algorithm
POST	Program to Optimize Simulated Trajectories
RCS	Reaction Control System
SGI	Silicon Graphics, Inc.
6DOF	Six degree-of-freedom
3DOF	Three degree-of-freedom
γ_i	Inertial Flight Path Angle, deg
θ	Spacecraft angular position
$\dot{\theta}$	Spacecraft angular rate

*Aerospace Engineer, Vehicle Analysis Branch, Space Systems and Concepts Division.
**Computer Analyst.
†ACS Engineer, Flight Systems
‡Engineer, Navigation and Flight Mechanics Section.

Introduction

The Mars Surveyor Program 2001 (MSP '01) Lander will utilize lift to perform precision landing, touching down within a 10-km radius of the science target [Ref. 1]. As originally conceived, the MSP '01 Orbiter design was based on an aerocapture strategy for Mars orbital insertion until budget problems resulted in a mission descope. Since the final configurations are evolving, only representative figures of the MSP '01 Lander and Orbiter systems are shown in Figs. 1 and 2, respectively. For each mission, autonomous control of the vehicle's atmospheric flight path would be required. Autonomous atmospheric lifting flight requires a propulsive control system to properly orient the vehicle lift vector and an atmospheric guidance algorithm to determine trajectory corrections and command the control system.

As a result of this increased emphasis on atmospheric flight, the MSP '01 mission formed an Atmospheric Flight Team (AFT) in August 1997. The objectives of this team were to develop: (1) aerocapture and precision landing strategies, (2) three- and six-degree-of-freedom atmospheric flight simulation testbeds, and (3) a broad set of potential atmospheric guidance algorithms. This guidance development activity is scheduled to conclude in September 1998 with downselection of a Lander guidance algorithm and the initiation of flight software production.

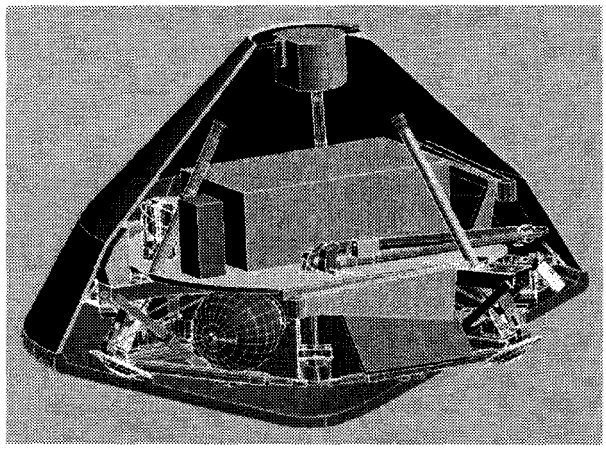

Fig. 1 Representative MSP '01 Lander Configuration.

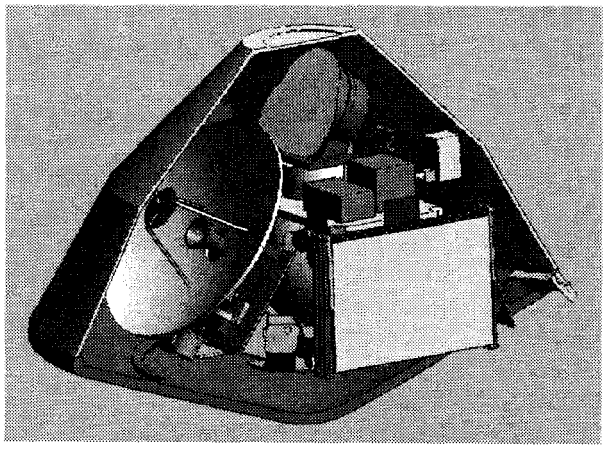

Fig. 2 Representative MSP '01 Orbiter Configuration.

The MSP '01 AFT was primarily composed of NASA and industry personnel from the Jet Propulsion Laboratory (JPL), Johnson Space Center (JSC), Langley Research Center (LaRC), and Lockheed-Martin Astronautics Co. (LMA) and reports directly to the MSP '01 Mission Manager. The simulation sub-group is responsible for development of the Project atmospheric flight simulation. As such, this group is comprised of the individuals with responsibility for development of the various models discussed in this paper. The AFT simulation is hosted on a Silicon Graphics, Inc. (SGI) platform at NASA LaRC. Once assembled, all members of the flight team have access to the simulation. The guidance subgroup is responsible for the development of a spectrum of guidance algorithms which will be evaluated by the AFT simulation. The deadline for submission of candidate guidance algorithms was Oct. 31, 1997. Seven Lander and six Orbiter candidate guidance algorithms were developed for evaluation. Development of several of these algorithms has been documented. [Refs. 2-6] Lander guidance algorithm downselection is scheduled for September 15, 1998.

To allow development and evaluation of candidate guidance algorithms for the MSP '01 Orbiter and Lander, three degree-of-freedom (3DOF) and six degree-of-freedom (6DOF) simulations were developed for each mission. These four simulations use the Program to Optimize Simulated Trajectories (POST) [Ref. 7] as the main simulation software, modified to include mission specific models. These models include the gravity, planet, atmosphere, aerodynamic data, control system, inertial measurement unit (IMU), and mass properties models. Figure 3 illustrates the basic flow of the AFT 6DOF testbed simulation. This figure also indicates the group responsible for each major model in the simulation. As seen in Fig. 4, the 3DOF simulations differ in that the Navigation and IMU models are combined, no propulsion model is used, and only translational equations of motion are integrated. The 3DOF simulations are used for guidance design and tuning by the Principal Investigator (PI) for that particular algorithm. The 6DOF simulations provide higher fidelity and include models that more accurately simulate the flight systems. These sim-

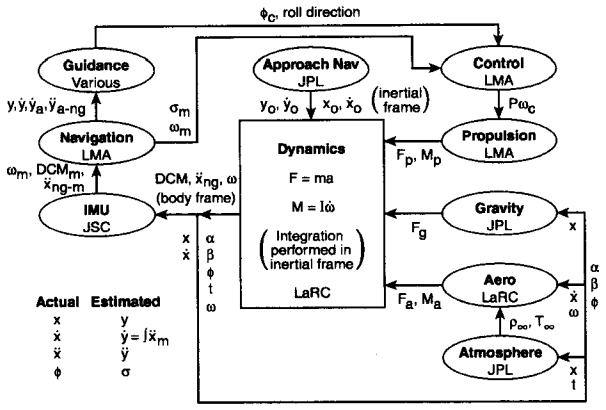

Fig. 3 MSP '01 six-degree-of-freedom atmospheric flight simulation.

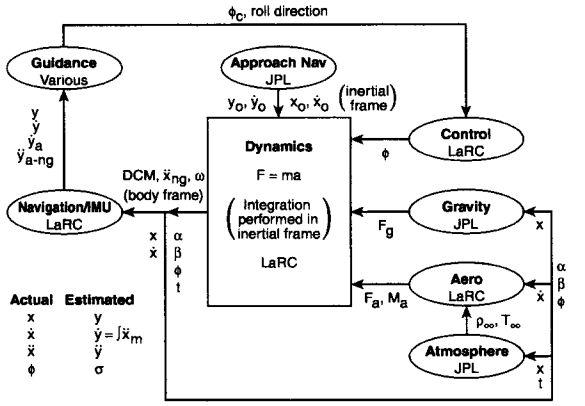

Fig. 4 MSP '01 three-degree-of-freedom atmospheric flight simulation.

ulations have been developed as the basis for Monte Carlo analyses of guidance algorithms proposed for both precision landing (MSP '01 Lander mission) and aerocapture (MSP '01 Orbiter mission). [Ref. 2-6]

This paper discusses the aspects of the four simulations that are unique to the MSP '01 mission analyses. The first section details the interface created to accept a wide variety of disparate guidance algorithms into the simulation. Next, mission specific models are presented, followed by the Monte Carlo setup including the variables to be dispersed and their range of values. Finally, the system analyses and outputs are discussed.

Guidance Algorithm Interface

A common interface is used between the simulations and the guidance algorithms. The data provided to the guidance algorithm included: (1) time since simulation start; (2) current estimate of vehicle bank angle; (3) current estimated vehicle inertial position and velocity vectors in Mars-centered Inertial (MCI) coordinates; (4) current sensed vehicle acceleration vector in MCI coordinates; (5) current estimated vehicle position, relative velocity, and relative acceleration vectors in Mars-centered Mars-fixed coordinates (MCMF); (6) current sensed acceleration in a Mars-atmospheric relative (ATM) coordinates; and (7) nine-element MCI to body and MCI to MCMF coordinate system transformation matrix.

The MCI coordinate system is an inertial, mean of epoch system with the origin at the center of Mars. That is, the MCI and MCMF coordinate axes are aligned at the beginning of the simulation. The primary (X-Y) plane for both the MCI and MCMF coordinate systems is the Mars equatorial plane, with the Z-axis out Mars north pole for both. The MCMF coordinate system also has its origin at the center of Mars, but it rotates with the planet such that its X-axis always passes through the Mars Prime Meridian. The ATM coordinate system is fixed to the spacecraft with the X-axis aligned with the spacecraft's Mars-relative velocity vector, and its Y-axis is the cross product of the MCMF relative velocity and position vectors. The body coordinate system is fixed to the spacecraft and has its X-axis aligned with the spacecraft's axis of symmetry.

The guidance algorithms were required to return the commanded bank angle and a rotation option flag. The rotation option flag specified one of five ways of achieving the commanded bank angle:

1) roll through the smallest angle necessary to reach the commanded angle;
2) roll in a positive sense toward the commanded angle;
3) roll in a negative sense toward the commanded angle;
4) roll continuously in a positive sense, ignoring the commanded angle;
5) roll continuously in a negative sense, ignoring the commanded angle.

Models

Several mission specific models were created or adjusted for use in POST for certain aspects of the simulation. These models include the gravity, planet, atmosphere, aerodynamic data, control system, IMU, and mass properties models. Additionally, the Mars 2001 project office provided an estimate of the delivery and knowledge states. Here, delivery state refers to the actual entry state; whereas, knowledge state refers to the best estimated state relayed to the vehicle (for navigation system initialization) five hours prior to the entry interface.

Gravity Model

The gravity model selected uses zonal, sectoral, and tesseral harmonic terms to determine the acceleration due to gravity. This model is based on the one used in the Artificial Satellite Analysis Program (ASAP). [Ref. 8] The MSP '01 Project Office provided data for a 50-by-50 Mars gravity field for use in these simulations. This gravity model was added to POST for use in all (3DOF and 6DOF, Orbiter and Lander) simulations.

Planet Model

An oblate spheroid Mars model is also used in all four simulations. This planet model defines the physical dimensions (e.g., equatorial radius, polar radius) and characteristics (e.g., rotation rate) of Mars. This model is not only used for altitude, latitude, and longitude determinations, but is also necessary to determine Mars relative velocity used by the guidance algorithms and other simulation models. For the Orbiter simulations, a reference spherical planet is used for apoapse and periapse altitude calculations only. The reference radius of this Mars model (denoted MRE) is shown in Table 1 along with the other Mars planetary model parameters used in the simulations.

Atmosphere Model

The Mars Global Reference Atmosphere Model [Ref. 9] version 3.7 (MarsGRAM 3.7) has been included in the simulations (as FORTRAN subroutines in POST). MarsGRAM provides all of the atmospheric data (temperature, density, pressure, and wind velocity) as well as random perturbations to certain atmospheric quantities (e.g., density). The atmospheric data is a function of the spacecraft location (latitude, longitude, and altitude) as well as other user supplied inputs. [Ref. 10] As shown in Table 2, these inputs include the date of Mars arrival, the minimum update distance dispersion calculations, a scale factor on the atmospheric dispersions, climate factor curve fit constants, interpolation option for the upper atmosphere, and the f10.7-cm solar flux value. The Mars arrival date and f10.7-cm solar flux values reflect the period during the solar cycle in which the entry occurs. A scale factor was used by the AFT to increase the magnitude of density perturbations which the guidance algorithms must accommodate. The climate factor curve fits were adjusted to better emulate the expected atmospheric conditions based on Global Circulation Models (GCM) data. The interpolation option establishes which methodology is used to extend the atmospheric data from the last climate factor curve fit constant. The nominal values for these MarsGRAM inputs in the Orbiter and Lander simulations are given in Table 2. In this table, the MarsGRAM input variable name is included as a parenthetical entry beside the input description. The only difference between the Lander and Orbiter atmosphere models are those due to time, date, latitude and longitude of entry, specifically the date and climate factors. Note that the same atmospheric model is used in the 3DOF and 6DOF simulations.

The MarsGRAM subroutine was selected as the atmospheric model for consistency with other MSP missions (e.g., Pathfinder, Mars Global Surveyor '98). In addition, since MarsGRAM is a parameterization of the atmospheric properties, this model runs relatively quickly so the overall simulation speed is not hampered by the atmospheric subroutine. Recent versions of MarsGRAM include "climate factors" which are adjusted to force the MarsGRAM density profile to agree with density profiles from more detailed simulations using GCM being developed at the NASA Ames Research Center (by Robert Haberle and James Murphy) and at the University of Arizona (by Steve Bougher). The climate factors allowed MarsGRAM to reproduce the more realistic densities from the GCM for a specific entry profile in the simulation but in a fraction of the time. Although MarsGRAM has the internal ability to approximate the effects of dust in the atmosphere, this option was not used. Instead, the climate factors were used to interpolate the effects of dust as seen in several different GCM simulations. Figures 3 and 4 show the comparison between density ratios generated from GCM and climate factor calculations for a nominal Orbiter and Lander entry trajectory. As noted in these figures, the general curvature of the profiles are maintained in the lower altitude regions (below 60 km

Table 1 Mars Planetary Model Parameters

Gravitational Parameter (μ)	$4.28282868534 \times 10^{13}$ m^3/sec^2
Equatorial Radius (r_E)	3393940 m
Polar Radius (r_P)	3376780 m
Mars Rotational Velocity (ω_{MARS})	7.088218×10^{-5} rad/sec
Mars Reference Radius (M_{RE})	3397200 m

Table 2 Mars GRAM Nominal Inputs

Orbiter Simulation	
Arrival Date	Julian Date 2452247.17365
Update Distance	0.5 km
Interpolation Option (ipopt)	hydrostatic interpolation (1)
Scale Factor (rpscale)	1.5
f10.7-cm Solar Flux (f107)	160.0
Climate Factor constant at surface (CF0)	1.0071012
Climate Factor constant at 5 km (CF5)	1.0355367
Climate Factor constant at 15 km (CF15)	1.090987
Climate Factor constant at 30 km (CF30)	1.06042
Climate Factor constant at 50 km (CF50)	0.8941667
Climate Factor constant at 75 km (CF75)	0.898953
Climate Factor constant for surface pressure (CFp)	0.98333
Lander Simulation	
Arrival Date	Julian Date 2452308.5
Update Distance	0.5 km
Interpolation Option (ipopt)	hydrostatic interpolation (1)
Scale Factor (rpscale)	1.5
f10.7-cm Solar Flux (f107)	160.0
Climate Factor constant at surface (CF0)	1.0051989
Climate Factor constant at 5 km (CF5)	0.988986
Climate Factor constant at 15 km (CF15)	1.008912
Climate Factor constant at 30 km (CF30)	1.00915
Climate Factor constant at 50 km (CF50)	0.873553
Climate Factor constant at 75 km (CF75)	0.8585096
Climate Factor constant for surface pressure (CFp)	0.76772

for the Lander and 80 km for the Orbiter simulation). The shape of the lower TAU curve in Fig. 2 matches very well as the higher altitudes are reached. A decision was made to keep a similar curvature for the higher TAU values, which results in a more conservative estimate of density in those regions for the Lander simulations.

A wrapper subroutine was developed to provide a software interface between the MarsGRAM program, developed by Jere Justus (through the NASA Marshall Space Flight Center) and the aerocapture simulation being developed at NASA Langley. The wrapper converts between the double precision variables used in the flight simulation and the single precision variables used by MarsGRAM. The wrapper program was designed to enable backward time steps while maintaining the random component that is available as an option in MarsGRAM. Since the only change made to the MarsGRAM code was the addition of a single common block to pass out several variables that were not included in the calling arguments, this wrapper should enable smooth updates as new versions of MarsGRAM become available.

Aerodynamic Model

A FORTRAN subroutine supplies aerodynamics to POST. The routine uses first derivative, or C(1), continuous interpolations between a database of discrete solutions. This interpolation scheme is applied to free molecular solutions for the rarefied region of the atmosphere, and computational fluid dynamic (CFD) solutions for the continuum regime. A modified Lockheed bridging function [Ref. 11] is used in the transitional region between rarefied and continuum regimes. The various flow regimes are delineated according to Knudsen number.

Entry capsules for robotic missions tend spend a considerable amount of time in rarefied and transitional flow regimes. Therefore, free molecular values are included in both aerodynamic databases. The aerodynamics in the rarified regime are a function of vehicle attitude. In the transitional regime, the aerodynamics are a function of both vehicle attitude and Knudsen number.

For the continuum region, static aerodynamic data were obtained from CFD solutions using the Langley Aerothermodynamic Upwind Relaxation Algorithm (LAURA) [Ref. 12-14]. LAURA was used to generate aerodynamic databases for the Mars Pathfinder [Ref. 15], Mars Microprobe [Ref. 11], and Stardust [Ref. 16] entry capsules. Confidence in the LAURA solutions comes from validations with Viking data, wind tunnel data, and Mars Pathfinder mission results. [Ref. 17] Dynamic aerodynamic quantities were included from the data generated for the Viking missions.

Some notable differences exist between the Lander and Orbiter aerodynamic models. The Orbiter aerocapture trajectory includes entry and egress through the free molecular and transitional regimes. Hence, two sets of free molecular solutions were done: one at entry velocity of 6600 m/sec and one at atmospheric exit velocity of 3500 m/sec. A total of 44 CFD solutions (angle of attack = 0,6,11.1,16 deg at 11 points along the trajectory) define the continuum aerodynamics for the Orbiter. The free molecular values for the Lander are based on a velocity of 6975 m/s. The continuum aerodynamics for the Lander consists of 52 CFD solutions (at 13 points along the trajectory) extending from the transitional regime down to Mach 2. For aerodynamic data in the continuum flow region, the Lander routine is a function of vehicle attitude and Mach number, whereas the Orbiter routine is a function of vehicle attitude and atmospheric relative velocity.

The 3DOF and 6DOF simulations utilize the same aerodynamic subroutine. However, the 3DOF simulation requires only C_A, C_N and C_m to satisfy the translational equations of motion and determine the trim angle of attack. The 6DOF simulations use all the force and moment information supplied by the aerodynamics routine. The aerodynamics for both the Orbiter and Lander were normalized using a reference length of 2.669 m and a reference area of 5.5948 m^2. The aerodynamic moment reference point is the nose.

Control System Model

As mentioned above, the guidance algorithms define the desired bank angle and mode to transfer to that angle. The control system model is responsible for executing these commands. The 6DOF simulation uses a control system model provided by the Lockheed Martin Astronautics Company, who is responsible for building the Mars 2001 spacecraft. This roll-axis bang-bang/limit cycle controller is based on the actual flight system. This flight model includes the four aft (pitch/yaw) and four roll thrusters planned for each spacecraft. The roll axis

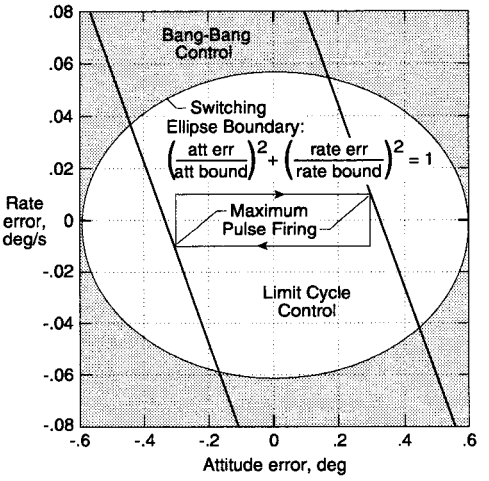

Fig. 7 Controller bounding ellipse (phase plane controller switching logic).

controller is designed to toggle between a bang-bang and a limit cycle controller based on a current attitude error and rate error. Figure 7 shows the bounding ellipse used to determine the type of controller to use.

When the attitude and rate errors are inside the ellipse, a limit cycle controller is used. The limit cycle controller is set up such that no thruster firings are commanded until the torque command from the controller is above a certain specified limit. Once the torque command reaches the specified limit, the thrusters are commanded to fire at a maximum impulse bit to change the direction of the spacecraft. Nominally, limit cycle control would involve firing minimum impulse bits to decrease fuel usage and allow for tighter deadbanding control. However, in the presence of atmosphere, the rate deadbands and angle deadbands have been widened to allow for oscillations in aerodynamic equilibrium without having the controller try to counteract the aerodynamic torques. The thruster pulsewidths are set at the maximum impulse bit in order to overcome aerodynamic torques if the spacecraft deviates too far from the desired attitude.

When the attitude and rate errors are outside the bounding ellipse, the controller switches to a bang-bang controller, which minimizes spacecraft recovery time. The spacecraft will switch to the bang-bang controller mostly in the event of a roll command, in which the reference attitude is adjusted to reflect a roll command of a given number of degrees as calculated by the guidance algorithm. A classical bang-bang control is single axis, and is designed to minimize peak error and time to reach steady-state by applying full acceleration towards zero error and then applying full deceleration to get the space-

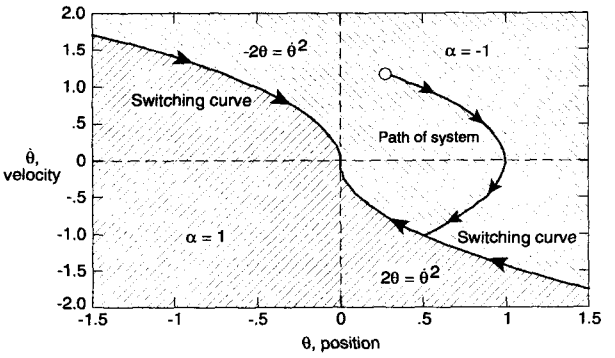

Fig. 8 Minimum time solution for single-axis bang-bang control (phase plane of system trajectory).

craft to stop at zero attitude error. Figure 8 illustrates the minimum time solution in the phase-plane region. With the acceleration constrained to be $|\alpha| = 1$, the switching lines are described by

$$\dot{\theta}^2 = \pm 2\theta$$

where θ and $\dot{\theta}$ represent the angular position and rate of the spacecraft, respectively. From Fig. 8, the normalized acceleration can be determined. This acceleration is converted into maximum thrust by a gain. For the MSP '01 Orbiter simulation, the bang-bang controller has been modified to limit the rate of the spacecraft to assist in the guidance algorithm. If the current spacecraft rate is above a set limit and the current commanded torque will increase the current rate, no command is sent to the thrusters.

The controller is also responsible for pitch and yaw control. The control system is commanded to follow the spacecraft trim angle of attack for a nominal entry profile. The commanded sideslip angle is zero. The pitch and yaw axes for the spacecraft employ the limit-cycle control only as specified in the roll control.

Additionally, the controller uses gain scheduling. For aerocapture, the controller goes through a series of gains based on the ground-relative velocity magnitude of the spacecraft. The number of gain changes is a programmable number (presently set to allow a maximum of six sets of gains). The present control strategy uses three sets of gains (2 gain changes). The controller begins with tight pointing in all 3 axes when negligible atmosphere is present, then switches to rate damping in the pitch and yaw axes and tight control about the roll axis when the atmosphere becomes dense enough to produce aerodynamic torques on the vehicle. This strategy relies on the use of aerodynamic torques to stabilize the pitch and yaw axes, and precisely controls the roll axis, thus providing a significant savings of fuel resulting from reduced thruster firings in pitch and yaw. When the atmosphere again becomes rarefied, the controller switches back to tight pointing control about all three axes. The atmospheric density has been correlated to the ground-relative velocity magnitude from which the gain change trigger values were derived. Only one gain set is used in the Lander simulation.

The 3DOF simulation uses a simplified bank rate, bank acceleration model to imitate the 6DOF control system. This model assumes a constant (maximum) bank acceleration is applied in the desired direction until the bank rate limit is reached, followed by a constant (maximum) bank deceleration to the desired bank angle. In the case of a continuous roll command, this model assumes a constant (maximum) acceleration until the maximum roll rate is reached, at which point the maximum roll rate is used until continuous roll is no longer commanded.

Inertial Measurement Unit

The Inertial Measurement Unit (IMU) model [Ref. 18] provides estimates of errors due to IMU systems which were applied to the data provided to the control system and used for state estimation and guidance command determination. This model determines random IMU perturbations based on a user supplied seed value. The 3DOF simulation used the IMU model in the navigation subroutine indicated below.

In the 6DOF simulation, estimates of the vehicle state are maintained as part of the control system based on the initial knowledge state estimate and the elapsed time on the atmospheric trajectory. For the 3DOF simulation, an estimated state is propagated in a navigation subroutine originally developed for POST by the Charles Stark Draper Laboratory, Inc. [Ref. 19] In this paper, these estimated states and the quantities derived from them are prefixed with the acronym NAV; whereas, the simulation states and their related quantities are referred to as actual values.

Mass Properties

The mass properties used for these simulations were the best estimates of the respective systems. Table 3 and 4 indicate the mass properties applied in the Orbiter and Lander simulations. The longitudinal center of gravity (cg) is measured from the spacecraft nose aft along the axis of symmetry. The lateral cg was selected to provide a lift-to-drag ratio (L/D) of about 0.18 for the Orbiter and 0.12 for the Lander in the peak dynamic pressure region of the atmospheric trajectory.

Table 3 Orbiter Mission Dispersions

Quantity	3 DOF	6 DOF	Nominal Value	Distribution Type	3-σ or min/max
Mission Uncertainty					
Initial Bank, deg	•	•	0.0	Gaussian	5.0
Initial Angle of Attack, deg		•	-14.7	Gaussian	5.0
Initial Sideslip Angle, deg		•	0.0	Gaussian	5.0
Initial Pitch rate, deg/sec		•	0.0	Gaussian	5.0
Initial Roll rate, deg/sec		•	0.0	Gaussian	5.0
Initial Yaw rate, deg/sec		•	0.0	Gaussian	5.0
Aerodynamic Uncertainty					
Axial Force Coeff Incr ($K_n \geq 0.1$)	•	•	0	Gaussian	10 %
Normal Force Coeff Incr ($K_n \geq 0.1$)	•	•	0	Gaussian	10 %
Axial Force Coeff Incr (Mach > 10)	•	•	0	Gaussian	3 %
Normal Force Coeff Incr (Mach > 10)	•	•	0	Gaussian	5 %
Axial Force Coeff Incr (Mach < 5)	•	•	0	Gaussian	10 %
Normal Force Coeff Incr (Mach < 5)	•	•	0	Gaussian	8 %
Pitch Moment Coeff Incr ($K_n \geq 0.1$)		•	0	Gaussian	10 %
Pitch Moment Coeff Incr (Mach > 10)		•	0	Gaussian	8 %
Pitch Moment Coeff Incr (Mach < 5)		•	0	Gaussian	10 %
Pitch Damping Coeff Incr (Mach > 10)		•	0	Gaussian	15 %
Pitch Damping Coeff Incr (Mach < 5)		•	0	Gaussian	15 %
Trim Angle of Attack Incr, deg	•		0	Gaussian	2.0
Mass Property Uncertainty					
Mass, kg	•	•	583.0	Gaussian	2.0
Axial CG position, m	•	•	0.7405	Gaussian	0.010
Lateral CG position, m	•	•	0.0339	Gaussian	0.005
Lateral CG offset direction, deg	•	•	0	Uniform	0/180
Ixx, kg-m^2		•	306.0	Gaussian	5 %
Iyy, kg-m^2		•	218.6	Gaussian	5 %
Izz, kg-m^2		•	244.0	Gaussian	5 %
Ixy, kg-m^2		•	0.0	Gaussian	3.0
Ixz, kg-m^2		•	0.0	Gaussian	3.0
Iyz, kg-m^2		•	0.0	Gaussian	3.0
Atmospheric Uncertainty					
Initial Seed Value	•	•	0	Uniform	1/29999
Update distance, km	•	•	0.5	Uniform	0.5/5.0
TAU	•	•	1.0	Uniform	0.3/1.6
Control System Uncertainty					
Bank Acceleration, deg/sec^2	•		7.40	Uniform	4.85/11.30
Roll/yaw thrusters (overall), lb		•	4.5	Uniform	3.0/7.0
Roll/yaw thrusters (relative)		•	0	Gaussian	5 %
Pitch thrusters (overall), lb		•	3.4	Uniform	2.3/5.3
Pitch thrusters (relative)		•	0	Gaussian	5 %
IMU Uncertainty					
Initial Seed Value		•	0	Uniform	1/29999
Initial angular misalignment, arcsec		•	0	Gaussian	126
Gyro bias drift, deg/hr		•	0	Gaussian	0.03
Gyro scale factor, ppm		•	0	Gaussian	99
Gyro nonorthogonality, ppm		•	0	Gaussian	60
Gyro random walk (PSD), deg/rt-hr		•	0	Gaussian	0.03
Accelerometer bias, milligees		•	0	Gaussian	0.18
Accelerometer scale factor, ppm		•	0	Gaussian	300

Table 4 Lander Mission Dispersions

Quantity	3 DOF	6 DOF	Nominal Value	Distribution Type	3-σ or min/max
Mission Uncertainty					
Initial Bank, deg	•	•	0.0	Gaussian	5.0
Initial Angle of Attack, deg		•	-14.7	Gaussian	5.0
Initial Sideslip Angle, deg		•	0.0	Gaussian	5.0
Initial Pitch rate, deg/sec		•	0.0	Gaussian	5.0
Initial Roll rate, deg/sec		•	0.0	Gaussian	5.0
Initial Yaw rate, deg/sec		•	0.0	Gaussian	5.0
Aerodynamic Uncertainty					
Axial Force Coeff Incr ($K_n \geq 0.1$)	•	•	0	Gaussian	10 %
Normal Force Coeff Incr ($K_n \geq 0.1$)	•	•	0	Gaussian	10 %
Axial Force Coeff Incr (Mach > 10)	•	•	0	Gaussian	3 %
Normal Force Coeff Incr (Mach > 10)	•	•	0	Gaussian	5 %
Axial Force Coeff Incr (Mach < 5)	•	•	0	Gaussian	10 %
Normal Force Coeff Incr (Mach < 5)	•	•	0	Gaussian	8 %
Pitch Moment Coeff Incr ($K_n \geq 0.1$)		•	0	Gaussian	10 %
Pitch Moment Coeff Incr (Mach > 10)		•	0	Gaussian	8 %
Pitch Moment Coeff Incr (Mach < 5)		•	0	Gaussian	10 %
Pitch Damping Coeff Incr (Mach > 10)		•	0	Gaussian	15 %
Pitch Damping Coeff Incr (Mach < 5)		•	0	Gaussian	15 %
Trim Angle of Attack Incr, deg	•		0	Gaussian	2.0
Mass Property Uncertainty					
Mass, kg	•	•	523.0	Gaussian	2.0
Axial CG position, m	•	•	0.7155	Gaussian	0.010
Lateral CG position, m	•	•	0.0170	Gaussian	0.005
Lateral CG offset direction, deg	•	•	0	Uniform	0/180
Ixx, kg-m^2		•	261.0	Gaussian	5 %
Iyy, kg-m^2		•	194.4	Gaussian	5 %
Izz, kg-m^2		•	212.3	Gaussian	5 %
Ixy, kg-m^2		•	0.0	Gaussian	1.0
Ixz, kg-m^2		•	0.0	Gaussian	3.0
Iyz, kg-m^2		•	0.0	Gaussian	15.0
Atmospheric Uncertainty					
Initial Seed Value	•	•	0	Uniform	1/29999
Update distance, km	•	•	0.5	Uniform	0.5/5.0
TAU	•	•	1.0	Uniform	0.3/1.6
Control System Uncertainty					
Bank Acceleration, deg/sec^2	•		1.78	Gaussian	0.178
Roll/yaw thrusters, lb		•	1.0	Gaussian	5 %
Pitch thrusters, lb		•	5.2	Gaussian	5 %
IMU Uncertaintiy					
Initial Seed Value		•	0	Uniform	1/29999
Initial angular misalignment, arcsec		•	0	Gaussian	126
Gyro bias drift, deg/hr		•	0	Gaussian	0.03
Gyro scale factor, ppm		•	0	Gaussian	99
Gyro nonorthogonality, ppm		•	0	Gaussian	60
Gyro random walk (PSD), deg/rt-hr		•	0	Gaussian	0.03
Accelerometer bias, milligees		•	0	Gaussian	0.18
Accelerometer scale factor, ppm		•	0	Gaussian	300

Termination Model

The Orbiter simulations ended when the spacecraft effectively departed the atmosphere. The AFT defined the end of the appreciable atmosphere at a radius of 3522.2 km. The simulation terminated when this radius was reached during the exit portion of the atmospheric trajectory. At that point, orbital elements and the delta-V to circularize into a 400 km orbit were determined for both the actual and NAV states.

The Lander simulations began the terminal phase when the parachute deploy conditions were attained. These conditions are based on an altitude and Mars-relative velocity criteria. The altitude must be between 13.5 and 6.5 km. While the altitude is between those values, the parachute deploys as soon as the velocity reaches 503.8 m/sec. If the velocity is less than 503.8 m/s when the altitude reaches 13.5 km, parachute deployment is at that upper limit. If the velocity is still greater than 503.8 m/sec at 6.5 km altitude, the simulation begins parachute deployment at the lower altitude limit. Note that the NAV altitude and velocity (estimated from models of onboard systems) were used to determine when the parachute deployment criteria were met. The guidance algorithms stop commanding vehicle attitude after parachute deployment. Thus, the results presented in Refs. 2-6 are for this parachute deploy location (longitude, geodetic latitude and altitude).

As part of the AFT testbed, a 3DOF simulation with a parachute model is included from the deploy location to touchdown at 2.5 km actual altitude. This simulation uses all of the basic models, not needed for the guidance algorithms, indicated above (atmosphere, mass properties, planet, gravity, and aerodynamic models). Starting from the deploy position and velocity, this terminal simulation invokes the parachute model which has an inflation rate required to reach the final parachute diameter of 13 m in about two seconds for a nominal entry. The simulation continues unguided using a parachute drag coefficient of 0.41. These parachute parameters were determined from Mars Surveyor '98 Lander and Mars Pathfinder mission studies. The final touchdown location was determined by ending the simulation when the actual altitude reached 2.5 km.

Entry State

Entry states were generated by JPL using the best estimate of interplanetary navigation errors, interplanetary trajectory correction maneuver errors, and the Earth departure window for each mission. Corresponding knowledge states at the atmospheric interface were also generated for each entry. These knowledge states are based on data available up to five hours prior to entry interface.

Monte Carlo Dispersions

The guidance algorithms were tested by varying several simulation models including the atmosphere, aerodynamic data, mass properties, control system, IMU, and initial states. The dispersed quantities were varied using either a uniform or gaussian distribution. Table 3 summarizes the dispersions used for the Orbiter simulations, while Table 4 includes those for the Lander simulations. The three-sigma (3-σ) values for the gaussian quantities or the bounding values of the uniformly distributed variables are given in these tables.

The atmospheric dispersion used in both the 3DOF and 6DOF simulations include the climate factor curve fits and distance between updates of the atmosphere. Curve fits of the climate factor (CF) constants simulate the effect on density of various levels of airborne dust particles. These curve fits are a function of the parameter TAU and are given in Table 5 for both the Orbiter and Lander simulations. These CF values are dispersed based on a uniform distribution of TAU between 0.3 and 1.6. In addition, the minimum distance along the trajectory between calls to MarsGRAM for updated atmospheric parameters was varied uniformly between 0.5 and 5.0 km. A uniformly distributed initial seed value between one and 29999 is also provided to the MarsGRAM subroutine for the additional density perturbations provided by that routine.

Aerodynamic uncertainties are determined for three regions of flight: rarified flow, Mach number above 10, and Mach number below five. Blending functions based on Mach or Knudsen number are used between these regions. Tables 3 and 4 indicate the aerodynamic coefficient increments, their distribution type (gaussian or uniform) and which dispersion analysis uses each quantity. These dispersions were applied at the aerodynamic reference point. For the 3DOF simulation, only force coefficient uncertainties were used (the normal force increment was also applied to the side force coefficient). In addition, for the 3DOF simulation, a uniformly distributed value (between ± 2 deg) was added to the trim angle of attack determined using unperturbed force and moment coefficient values. This dispersion was included as a means of modeling 6DOF issues. Note that in the 6DOF simulation the pitching moment and pitch damping coefficient increments were also applied to the yawing moment and yaw damping coefficients, respectively.

Table 5 Climate Factor Curve Fit Functions

Orbiter Simulation	
Climate Factor constant at Surface (CF0)	= 1.01400 – 0.0068988 * TAU
Climate Factor constant at 5 km (CF5)	= 1.02560 + 0.0099367 * TAU
Climate Factor constant at 15 km (CF15)	= 1.04200 + 0.0489870 * TAU
Climate Factor constant at 30 km (CF30)	= 0.83125 + 0.2291700 * TAU
Climate Factor constant at 50 km (CF50)	= 0.90250 – 0.0083333 * TAU
Climate Factor constant at 75 km (CF75)	= 0.97187 – 0.0729170 * TAU
Climate Factor constant for surface pressure (CFp)	= 0.65000 + 0.3333300 * TAU
Lander Simulation	
Climate Factor constant at Surface (CF0)	= 1.01290 – 0.0077011 * TAU
Climate Factor constant at 5 km (CF5)	= 0.95753 + 0.0314560 * TAU
Climate Factor constant at 15 km (CF15)	= 0.94510 + 0.0638120 * TAU
Climate Factor constant at 30 km (CF30)	= 0.90674 + 0.1024100 * TAU
Climate Factor constant at 50 km (CF50)	= 0.79403 + 0.0795230 * TAU
Climate Factor constant at 75 km (CF75)	= 0.85103 + 0.0074796 * TAU
Climate Factor constant for surface pressure (CFp)	= 0.56121 + 0.2065100 * TAU

The dispersed mass property values are also given in Tables 3 and 4. As noted in these tables, the 3DOF simulations used only the cg and mass uncertainties. Whereas, the 6DOF simulations included the mass moments of inertia.

The control system dispersions are similar for both the Orbiter and Lander simulations, except for the thruster, and hence roll acceleration, values. For the Orbiter, the biggest impact on the control system is the large variation in the roll/yaw thrust depending on tank pressure at Mars arrival. As indicated in Table 3, this variation in overall roll/yaw thrust is modeled as a uniform distribution between 3.0 and 7.0 lb. The variation in tank pressure caused the pitch (also called aft) thrust to vary uniformly between 2.3 and 5.3 lb. Additionally, a five percent (3σ) thruster-to-thruster uncertainty was included. For the 3DOF simulation, the roll/yaw thruster variation was modeled as a uniform variation in maximum bank acceleration of between 4.85 and 11.30 deg/sec^2. For the Lander, only the five-percent thruster-to-thruster gaussian variation was used in the 6DOF simulation. This thruster uncertainty was characterized as a maximum bank acceleration of 1.78 deg/sec^2 with a 10% gaussian variation for the 3DOF Lander simulation.

The IMU variations are also given in Tables 3 and 4. Note that dispersions in these parameters were an integral part of the IMU subroutine. This routine requires an initial seed value input from which the dispersions on the IMU parameters are selected by the routine. As indicated in these tables, a uniformly distributed initial seed value between 1 and 29999 is used in the dispersion analyses.

The mission uncertainties include entry state, knowledge errors in that state, initial spacecraft attitude and attitude rate. Tables 3 and 4 show the initial attitude and attitude rates used in these dispersion analyses. Note that the 3DOF simulations only perturb the initial bank angle, whereas the 6DOF simulations include uncertainties in all the initial attitude angles. The same initial states and knowledge errors were used in both the 3DOF and 6DOF simulations for a given mission. At a reference radius of 3522.2 km from Mars, the Orbiter mission entry state has a mean inertial flight path angle (γ_i) of -11.13 deg with a maximum variation of $\pm$ 0.48 deg, an inertial velocity of 6706 $\pm$ 26 m/sec, and an azimuth (clockwise from north) of 18.20 $\pm$ 0.24 deg. The initial state knowledge error for the Orbiter mission has a maximum position error of 25000 m and maximum velocity error of 11.5 m/sec. For the Lander mission, the entry state (also at a reference 3522.2 km radius) has a mean γ_i of -14.50 deg with a maximum variation of $\pm$ 0.23 deg, an inertial velocity of 6973 $\pm$ 29 m/sec, and an azimuth of 101.56 $\pm$ 0.09 deg. The Lander mission initial state knowledge error has a maximum position error of 15800 m and maximum velocity error of 6.1 m/sec.

Simulation Analyses/Outputs

Two thousand Monte Carlo input cases were generated for each of the four simulations based on dispersion values discussed above. Each PI was given access to the 3DOF and 6DOF simulation using their guidance algorithm and the first one hundred dispersed input cases for that particular mission. Using these dispersed cases, adjustments were made to the algorithms until the AFT

imposed stop date in July 1998. At that time, the two thousand cases were run and results were generated for the various guidance methodologies. [Refs. 2-6]

Similar output is provided by both the 3DOF and 6DOF simulations. For the Lander simulation, the range from the guidance PI determined parachute deployment target point is determined using both the actual and NAV states. The latitude, longitude, and altitude (from both the actual and NAV states) at the end of the simulation are also recorded. The Mach number and dynamic pressure are stored when the parachute deploys. The reaction control system (RCS) propellant usage as calculated in the control system subroutines is determined in the 6DOF simulation only.

Outputs for the Orbiter simulation include the apoapse and periapse of the orbit upon exiting the atmosphere. These apsides are indicated as altitudes above a reference sphere of radius 3397.2 km. In addition, these quantities are calculated using the actual and NAV states. Further outputs generated using both states included the exit orbit inclination and longitude of ascending node, as well as the velocity increment (delta-V) necessary to circularize the orbit at 400 km altitude above the reference sphere. Again, the RCS propellant from control system calculations is included for the 6DOF simulation.

Several outputs were common to all four simulations. These outputs included the maximum deceleration during the atmospheric trajectory. Also included were the maximum heat rate (based on the Sutton-Graves equation at Mars) and the total heat load as integrated from the calculated heat rate.

Closing Remarks

In summary, four simulations were developed in support of the MSP '01 Lander and Orbiter atmospheric guidance algorithm design, development, testing, and evaluation activities of the Atmospheric Flight Team. These two 3DOF and two 6DOF testbed simulations use POST as the basic simulation engine and include aerodynamic data, atmosphere, control system, IMU, planet, gravity, and mass property models provided by AFT team members. These simulations have been developed as the basis for Monte Carlo analyses of proposed MSP '01 precision landing and aerocapture guidance algorithms.

References

1. Braun, R.D., Spencer, D.A., Carpenter, J.R., and Willcockson, W.H.; "Mars Precision Landing," IAF 98-Q.3.03, 49th International Astronautical Congress, Sept. 28 - Oct. 2, 1998, Melbourne, Australia.

2. Carman, G.L., and Ives, D.G. "Apollo-Derived Precision Lander Guidance," Paper No. 98-4570, AIAA Atmospheric Flight Mechanics Conference, Boston, MA, August 1998.

3. Ro, T.U. and Queen, E.M. "Mars Aerocapture Terminal Point Guidance and Control," Paper No. 98-4571, AIAA Atmospheric Flight Mechanics Conference, Boston, MA, August 1998.

4. Bryant, L.E., Tigges, M., and Iacomini, C. "Analytic Drag Control for Precision Landing and Aerocapture," Paper No. 98-4572, AIAA Atmospheric Flight Mechanics Conference, Boston, MA, August 1998.

5. Tu, K.-Y., Munir, M., Mease, K., and Bayard, D. "Drag-Based Predictive Tracking Guidance for Mars Precision Landing," Paper No. 98-4573, AIAA Atmospheric Flight Mechanics Conference, Boston, MA, August 1998.

6. Powell, R.W., Willcockson, W., and Johnson, M.A. "Numerical Predictor Corrector Aerocapture and Precision Landing Guidance Algorithms for the Mars 2001 Missions," Paper No. 98-4574, AIAA Atmospheric Flight Mechanics Conference, Boston, MA, August 1998.

7. Bauer, G.L., Cornick, D.E., and Stevenson, R. "Capabilities and Applications of the Program to Optimize Simulated Trajectories (POST)," NASA CR-2770, February 1977.

8. Kwok, J.H. "The Artificial Satellite Analysis Program (ASAP) Version 2.0", JPL EM 312/87-153, 20 April 1987.

9. Justus, C.G., "Mars Global Reference Atmospheric Model for Mission Planning and Analysis", *Journal of Spacecraft and Rockets*, Vol. 28, No. 2, pp. 216-221, April-June 1991.

10. Justus, C.G., James, B.F., and Johnson, D.L., "Recent and Planned Improvements in the Mars Global Reference Atmospheric Model (Mars-GRAM)", Advances in Space Research, Vol. 19, No. 8, pp. 1223-1231, 1997.

11. Mitcheltree, R.A., Wilmoth, R.G., Cheatwood, F.M., Brauckmann, G.J., Greene, F.A., "Aerodynamics of Stardust Sample Return Capsule," AIAA Paper 97-2304, 15th Applied Aerodynamics Conference, Atlanta, GA, June 23-25, 1997.

12. Gnoffo, P.A., Gupta, R.A., and Shinn, J.L., "Conservation Equations and Physical Models for Hypersonic Air Flows in Thermal and Chemical Nonequilibrium," NASA TP-2867, Feb. 1989.

13. Cheatwood, F.M. and Gnoffo, P.A., "User's Manual for the Langley Aerothermodynamic Upwind Relaxation Algorithm (LAURA)," NASA TM 4674, April 1996.

14. Riley, C.J. and Cheatwood, F.M., "Distributed-Memory Computing with the Langley Aerothermodynamic Upwind Relaxation Algorithm (LAURA)," Proceedings of the 4th NASA National Symposium on Large-Scale Analysis and Design on High-Performance Computers and Workstations, Williamsburg, VA, October 15-17, 1997.

15. Gnoffo, P.A., Weilmuenster, K.J., Braun, R.D., and Cruz, C.I., "Influence of Sonic-Line Location on Mars Pathfinder Probe Aerothermodynamics," Journal of Spacecraft and Rockets, Vol. 33, No. 2, March-April 1996.

16. Mitcheltree, R.A., Moss, J.N., Cheatwood, F.M., Greene, F.A., and Braun, R.D., "Aerodynamics of the Mars Microprobe Entry Vehicles," AIAA Paper 97-3658, Atmospheric Flight Mechanics Conference, New Orleans, LA, August 11-13, 1997.

17. Gnoffo, P.A., Braun, R.D., Weilmuenster, K.J., Powell, R.W., Mitcheltree, R.A., and Engelund, W.C., "Prediction and Validation of the Mars Pathfinder Aerodynamic Database," AIAA Paper 98-2445, June 1998.

18. Carpenter, J.R., "Delivery of Inertial Measurement Unit Model to Mars Surveyor '01 Atmospheric Flight Team," NASA Johnson Space Center Memorandum EG-97-103, Sept. 26, 1997.

19. Kreimendahl, F.A. and Kriegsman, B.A. "User's Guide for the CSDL Navigation-System Simulator", The Charles Stark Draper Laboratory, Inc., December 1986.